ENDOR investigation of cubic Fe^{3+} centres in NaCl single crystals

1995 J. Phys.: Condens. Matter 7 2225

(http://iopscience.iop.org/0953-8984/7/10/028)

J. Phys.: Condens. Matter 7 (1995) 2225–2235. Printed in the UK

ENDOR investigation of cubic Fe^{3+} centres in NaCl single crystals

S V Nistor†, Th Pawlik and J-M Spaeth

University of Paderborn, Fachbereich 6-Physik, Warburger Strasse 100A, D–33098 Paderborn, Germany

Received 29 November 1994

Abstract. Cubic Fe^{3+} centres in NaCl single crystals have been studied with electron nuclear double resonance (ENDOR) at $T = 17$ K. The superhyperfine (SHF) and quadrupole interactions of the paramagnetic ion with the nearest set of four Cl^- anions and the second-nearest set of twelve Na^+ cations have been determined. The results confirm the structural model of an Fe^{3+} ion at a tetrahedrally symmetric interstitial position with the nearest four Na^+ cations missing, as suggested previously from the analysis of the SHF structure of their EPR spectra.

1. Introduction

It was shown by many electron paramagnetic resonance (EPR) studies that transition-metal ions are incorporated into alkali halide crystals substitutionally at cation sites, the extra positive charge being compensated by cation vacancies or anion impurities with an extra negative charge. The charge compensating vacancies or impurities are usually bound to the transition ion, inducing an axial or orthorhombic local crystal field component superimposed on the cubic crystal field of the undisturbed lattice (Sootha and Agarwal 1971, Narayana *et al* 1981).

It has been reported, however, that in NaCl crystals doped with iron an EPR spectrum due to Fe^{3+} ions at lattice sites with cubic symmetry is observed (Nistor and Velter-Stefanescu 1985). The corresponding Fe^{3+}_{cub} paramagnetic centres in NaCl doped with iron were obtained either by x-ray irradiation at room temperature, or by x-ray irradiation at $T = 80$ K followed by annealing above $T = 300$ K (Nistor *et al* 1987).

To explain the spectra it has been suggested (Nistor and Velter-Stefanescu 1985) that the Fe^{3+} ions are situated at tetrahedrally symmetric interstitial positions, with the four nearest-neighbour (NN) Na^+ ions missing. With this model it is possible to explain the compensation of the extra positive charge of Fe^{3+} and the cubic symmetry of the EPR spectrum. The proposed structural model was based on the similarity of the superhyperfine (SHF) structure of the central $m_s = \frac{1}{2} \leftrightarrow -\frac{1}{2}$ transition, observed with the magnetic field along the main crystallographic directions, with the previously reported one for the cubic Fe^{3+} centres in AgCl (Hayes *et al* 1964). The interstitial model of the cubic Fe^{3+} centre in AgCl has been confirmed beyond doubt by electron nuclear double-resonance (ENDOR) studies (Garth 1965, Satoh and Slichter 1966).

Compared to silver halides where interstitial cations are rather normal due to the predominance of the Frenkel type disorder, the presence of interstitial Fe^{3+} cations in

† Permanent address: Institute of Atomic Physics (IFTM), PO Box MG-6 Magurele, Bucuresti-76900, Romania.

0953-8984/95/102225+11$19.50

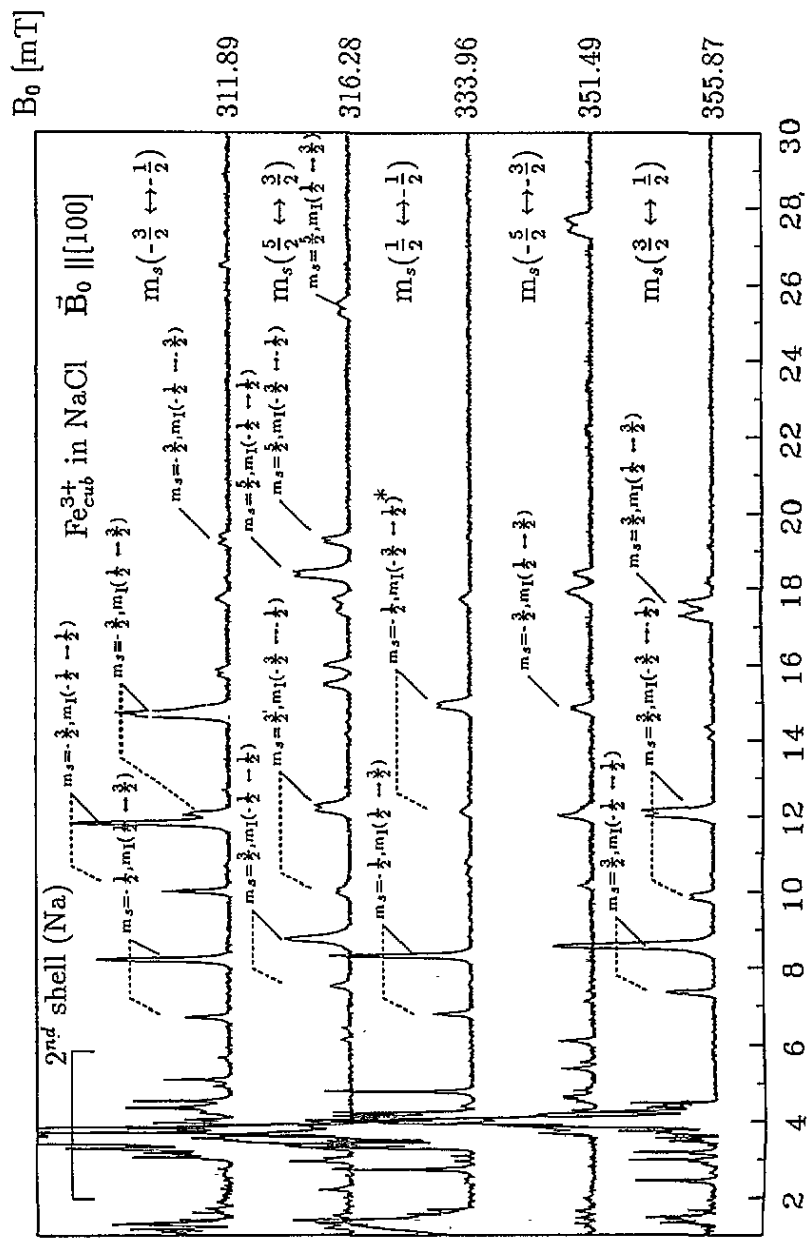
B0 [mT]
2nd shell (Na)
Fe3+cub in NaCl B0 ||[100]
311.89
316.28
333.96
351.49
355.87
2 4 6 8 10 12 14 16 18 20 22 24 26 28 30
frequency [MHz]
(a)

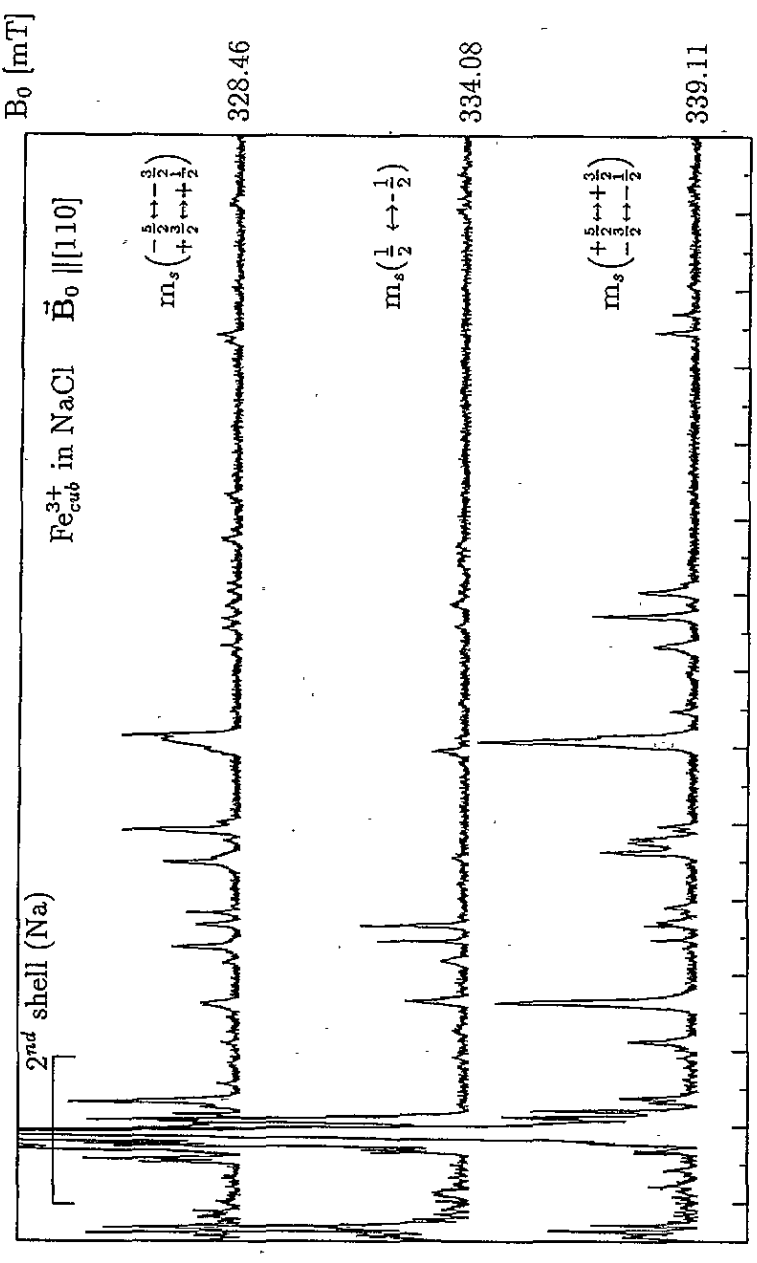

Figure 1. ENDOR spectra of the Fe^{3+}_{cub} centres in NaCl, obtained at $T = 17$ K by saturating the various EPR fine-structure transitions for (*a*) $B_0 \parallel [100]$ and (*b*) $B_0 \parallel [110]$. In all cases the smooth background signal has been substracted. The quantum states associated with the most representative transitions are indicated in (*a*). The solid lines indicate the ENDOR transitions from the ^{35}Cl isotope; the dashed lines indicate the transitions from the ^{37}Cl isotope. The lines marked (*) belong to forbidden ($\Delta m_I = 2$) ENDOR transitions.

alkali halides, where the cation defects are of Schottky type, represents a rather unexpected behaviour.

In view of the unusual character of this centre, as well as the fact that other structural models with tetrahedral symmetry, as suggested by Garth (1965), could not entirely be excluded, we undertook an ENDOR study of the Fe^{3+}_{cub} centres in NaCl with the main purpose of determining their structural model. Another interesting aspect was the possibility of comparing the transferred SHF interaction with the second cation shell in NaCl and AgCl to obtain more information about covalency effects in the AgCl lattice (Olm *et al* 1988).

2. Experimental details

The samples, of $4 \times 4 \times 15$ mm^3 size, were cleaved from the same NaCl single crystal which was used in the previous EPR studies (Nistor and Velter-Stefanescu 1985). The crystal was doped in the melt with iron and grown by the Bridgman technique in a chlorine atmosphere. The concentration of iron in the crystal lattice has been found by colorimetrical analysis to be in the 10^1–10^2 ppm range, the lower concentration being at the bottom of the crystal and the highest at the top. The sample was annealed at $T = 773$ K for 10 minutes in an alumina boat and quenched to room temperature on a metal block. After about $\frac{1}{2}$ hour the sample was inserted into a cryostat and kept below $T = 80$ K. The sample was then irradiated with x-rays (W anode, 60 kV, 15 mA) at $T = 80$ K for 1 hour. After irradiation the sample was annealed for 10 minutes at $T = 328$ K in an oven and inserted into the microwave cavity at $T = 80$ K. Such a procedure provides a complete conversion of the precursor non-cubic Fe^{3+} centres, produced by low-temperature irradiation (Nistor *et al* 1987), into the cubic Fe^{3+} centres, resulting in a higher concentration of those centres compared with the room-temperature x-ray irradiation.

The iron impurities are present as Fe^{2+} ions in NaCl and have a strong tendency to agglomerate, even at room temperature, as shown from a previous Mössbauer study on a similar crystal (Barb *et al* 1990). We estimate that only a few per cent of the total amount of iron is left in a dispersed state in the NaCl lattice by our sample handling procedure. However, that was enough to obtain strong EPR signals from the Fe^{3+}_{cub} centres after x-irradiation. EPR and stationary ENDOR experiments were performed with a custom built, computer controlled X band spectrometer. The sample temperature could be varied between 4 and 300 K and the ENDOR frequency could be varied between 300 kHz and 100 MHz. The best stationary ENDOR spectra were obtained at $T = 17$ K.

3. Results

EPR measurements at $T = 20$ K, with the magnetic field rotated in the (001) plane, confirmed the exclusive presence of Fe^{3+}_{cub} centres and allowed an accurate orientation of the crystal.

The ENDOR spectra were recorded on all five fine-structure split EPR transitions ($S = \frac{5}{2}$) for $B_0 \parallel [100]$ and $B_0 \parallel [110]$ (figures 1(a) and 1(b)). The angular dependence of the ENDOR spectra (figures 2 and 3) was recorded for the central quasi-isotropic EPR transition $m_s = +\frac{1}{2} \leftrightarrow -\frac{1}{2}$, observed at 334.1 mT (microwave frequency $\nu = 9.3979$ GHz).

The ENDOR spectra corresponding to the central $m_s = +\frac{1}{2} \leftrightarrow -\frac{1}{2}$ EPR transition are found in the 1–18 MHz range and can be considered as consisting of three main parts.

The first part, measured between 5 MHz and 18 MHz, contains ENDOR lines identified as being due to the interaction with the chlorine nuclei of the first shell (see figure 2).

A second group of intense, anisotropic lines in the 2.6–4.8 MHz range, identified as

being due to the interaction with the ^{23}Na nuclei ($I = \frac{3}{2}$, 100% abundant), is centered about the strong ENDOR transition at 3.76 MHz, the Larmor frequency of free ^{23}Na nuclei (see figure 3). The main group of anisotropic lines in this range belongs to the ^{23}Na nuclei of the second shell of cations.

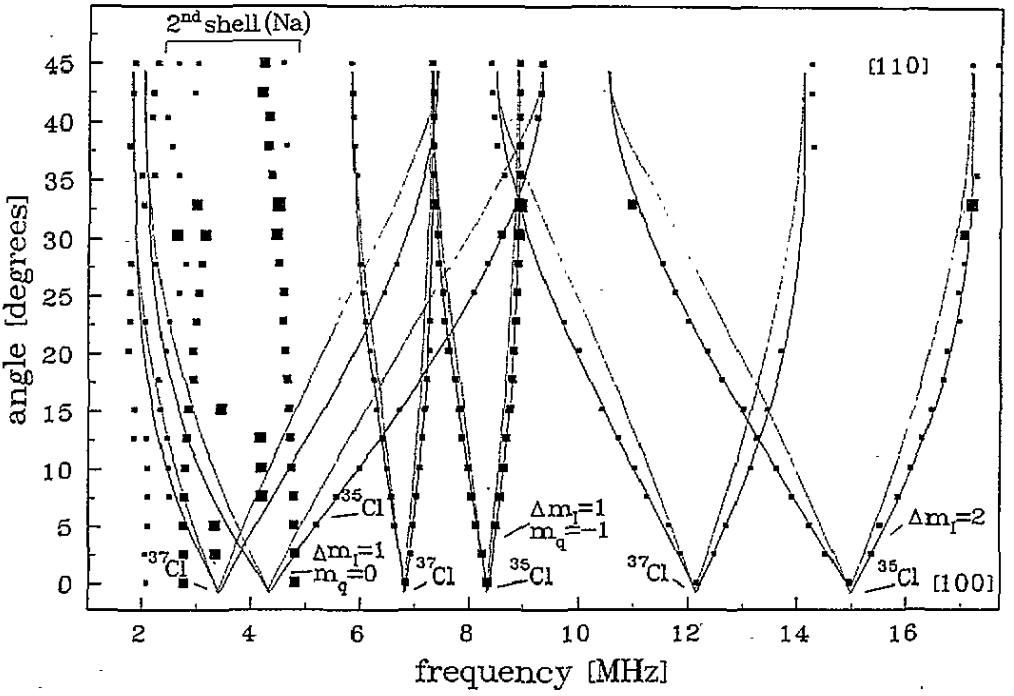

Figure 2. Angular dependence of the ^{35}Cl and ^{37}Cl ENDOR lines ($m_s = -\frac{1}{2}$ transition) from the interaction with the four Cl^- ligands of the first shell. The magnetic field B_0 is rotated in a (001) plane. Both the experimental data (dots) and the calculated angular dependence using the parameters given in table 1 are presented. The solid lines represent the final calculation, the dotted lines that without inclusion of the fine-structure interaction. m_q is defined as $(m_I+m'_I)/2$, where m_I and m'_I are the quantum numbers of the two energy levels involved in the NMR transition.

Several weak, strongly anisotropic ENDOR lines, in both frequency position and intensity, are observed at frequencies below 4.5 MHz. They can be attributed to the interaction with chlorine ligands situated further away from the Fe^{3+} ion. The most intense of these lines are observed around the Larmor frequencies of the ^{35}Cl (1.395 MHz) and ^{37}Cl (1.161 MHz) isotopes (the two Cl isotopes have abundances of 75.77% and 24.23%, respectively).

The ENDOR spectra were described quantitatively with the following spin-Hamiltonian:

$$\mathcal{H} = g\mu_B \boldsymbol{B}_0 \cdot \boldsymbol{S} + B_4(\hat{O}_4^0 + 5\hat{O}_4^4) + \sum_j (\boldsymbol{S}\hat{\boldsymbol{A}}_j\boldsymbol{I}_j + \boldsymbol{I}_j\hat{\boldsymbol{Q}}_j\boldsymbol{I}_j - g_{Ij}\mu_n \boldsymbol{B}_0 \cdot \boldsymbol{I}_j) \qquad (1)$$

with the usual notations (see e.g. Spaeth *et al* 1992). Here $S = \frac{5}{2}$, $I = \frac{3}{2}$ for ^{23}Na, ^{35}Cl and ^{37}Cl. The sum runs over the various Cl and Na ligands. The first term corresponds to the electronic Zeeman interaction, the second to the cubic fine-structure term and the last three denote the SHF, quadrupole and nuclear Zeeman interactions, respectively. The g and the fine-structure parameters were determined by EPR measurements (Nistor and Velter-Stefanescu 1985): $g = 2.0138$ and $B_4/h = 2.033$ MHz.

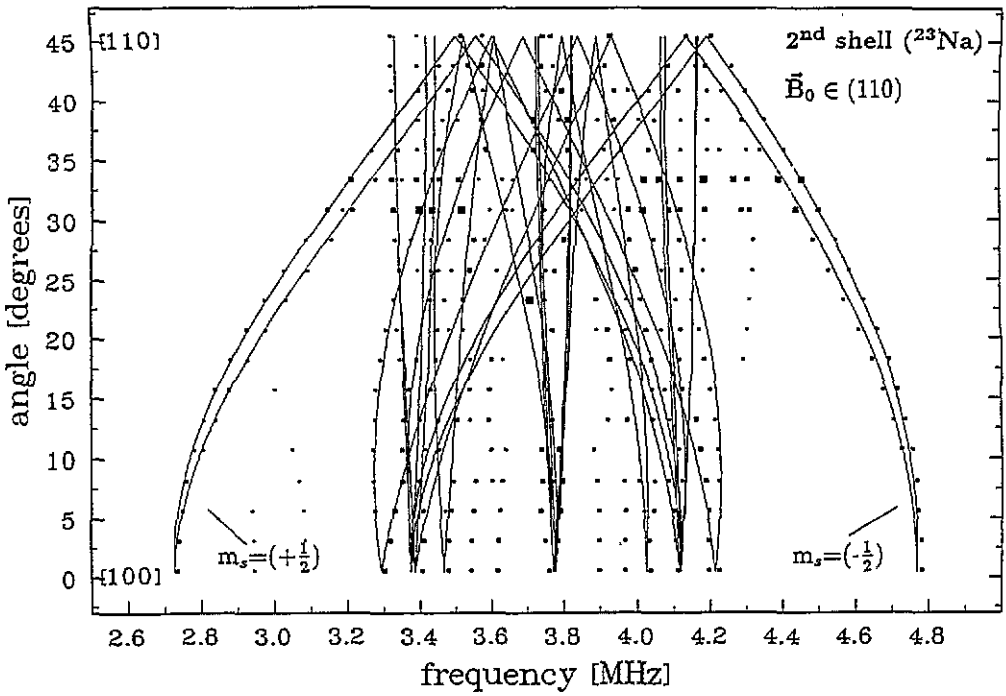

Figure 3. Angular dependence of the ^{23}Na ENDOR lines ($m_s = +\frac{1}{2}$ and $m_s = -\frac{1}{2}$ transitions) from the interaction with the second shell of ligands. The magnetic field B_0 is rotated in a (001) plane. The calculated angular dependence (continuous lines) was obtained with the parameters given in table 1, including the fine-structure term.

The structural model for which the ENDOR spectra could be explained is shown in figure 4. The Fe^{3+} ion is situated in an interstitial site of the NaCl lattice, at the centre of a regular tetrahedron of four Cl^- ions, representing the first shell of anion ligands. The ENDOR lines of ^{35}Cl and ^{37}Cl nuclei with the largest SHF interactions belong to a shell where the SHF and quadrupole interactions have axial symmetry about the [111] directions. Since the [111] directions are the connection lines between the interstitial Fe^{3+} and the nearest Cl and Na neighbours and threefold symmetry axes, for an interstitial Fe^{3+} such ENDOR lines are expected. Substitutional Fe^{3+} would have ^{35,37}Cl interactions with [100] symmetry axes. The four Na^+ ions from the first shell of cation ligands are missing, which is concluded from the absence of ENDOR lines from ^{23}Na nuclei with [111] symmetry.

A two-step procedure has been employed in the determination of the spin Hamiltonian parameters for the first shell. The first step consisted of a numerical diagonalization of the spin Hamiltonian (1) for the $m_s = +\frac{1}{2} \leftrightarrow -\frac{1}{2}$ transitions without consideration of the fine-structure terms. Due to the large quadrupole contribution both 'allowed' ($\Delta m_I = \pm 1$) and 'forbidden' ($\Delta m_I = \pm 2$) transitions were taken into consideration. The resulting ENDOR frequencies calculated for the various orientations were compared with the experimental ENDOR spectra. For an improved set of parameters the other ENDOR transitions for $|m_s| > \frac{1}{2}$ and $B_0 \parallel [100]$ were also taken into account.

It turned out that the fine-structure terms could not be neglected for orientations away from the [100] or [110] directions. The accurate explanation of the experimental line positions was achieved in a second step by taking this interaction into account, which was done by using the concept of the effective electron spin (for details see e.g. Spaeth *et al*

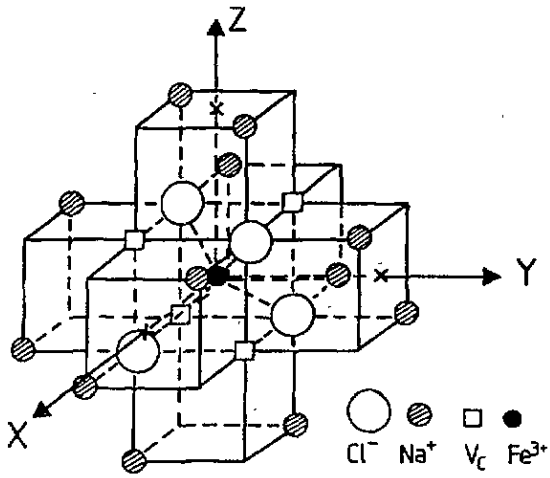

Figure 4. The structural model of the Fe^{3+}_{cub} centre in NaCl, as inferred from EPR studies and confirmed by the analysis of the ENDOR data. All ligands of the first shell and of the second shell of cations are represented. The ligand–Fe^{3+} ion distance for the first shell of ligands is $0.25d\sqrt{3}$, where $d = 0.55958$ nm is the lattice constant at $T = 4.2$ K. The second shell of ligands is represented by twelve Cl^- anions and twelve Na^+ cations situated at $0.5d\sqrt{11}$ from the Fe^{3+} ion in the unrelaxed NaCl lattice.

1992). In figure 2 the solid lines represent the final calculation, the dotted lines the angular dependence without inclusion of the fine-structure interaction.

The resulting SHF and quadrupole interaction parameters for the ^{35}Cl isotope are given in table 1, together with the corresponding data for the cubic Fe^{3+} centres in AgCl (Garth 1965, Satoh and Slichter 1966).

Table 1. SHF and quadrupole interaction constants (in MHz) of the Fe^{3+}_{cub} centre in NaCl, at $T = 17$ K. The angles Θ_S and Θ_Q of the SHF and quadrupole tensor orientations are defined in figure 5. The uncertainty of the parameters is one and six units on the last digit for the first and the second shell, respectively and two degrees for the angles. The SHF interaction constants of the Fe^{3+}_{cub} centre in AgCl (Garth 1965, Satoh and Slichter 1966) are also presented for comparison.

Host	Shell	Nucleus	a/h	b/h	b'/h	q/h	q'/h	Θ_S (deg)	Θ_Q (deg)
NaCl	I	^{35}Cl	8.444	1.195	0	1.812	0	0	0
NaCl	II	^{23}Na	0.218	0.181	0.086	0.125	0	−11	5.6
AgCl	I	^{35}Cl	8.40	1.57	0	1.91	0	0	0
AgCl	II	^{109}Ag	0.174	−0.148	−0.020	0	0	−2.7	0

They are given in terms of the isotropic SHF constant a and the anisotropic SHF constants b and b', which are related to the principal values of the SHF tensor by

$$A_{xx} = a - b + b' \qquad A_{yy} = a - b - b' \qquad A_{zz} = a + 2b. \tag{2}$$

In a similar way, the quadrupole interaction constants are related to the quadrupole tensor by

$$Q_{xx} = -q + q' \qquad Q_{yy} = -q - q' \qquad Q_{zz} = 2q. \tag{3}$$

For the first shell of Cl^- neighbours $b' = q' = 0$ due to the axial symmetry of the Fe^{3+}–Cl^- bond. In the case of the second shell the lower local symmetry requires that all parameters in (2) and (3) have to be considered.

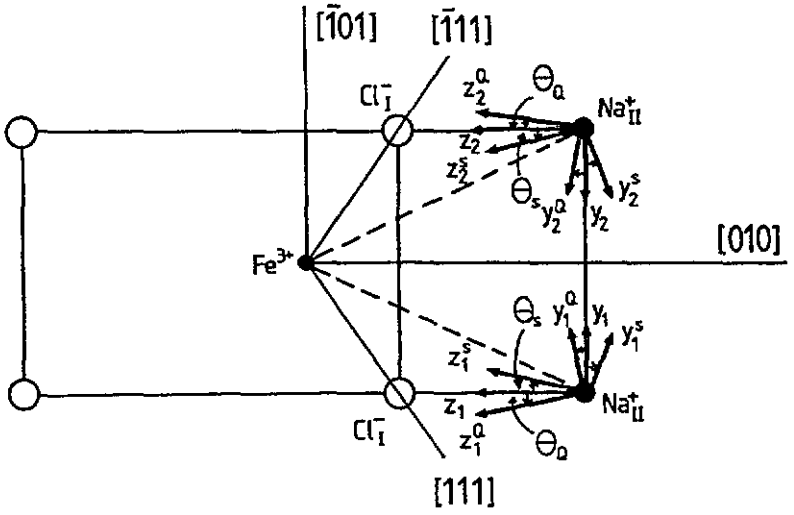

Figure 5. The orientation of the SHF (x_j^S, y_j^S, z_j^S) and quadrupole (x_j^Q, y_j^Q, z_j^Q) tensor principal axes associated to the ^{23}Na nuclei of the second shell of ligands, with respect to the local frame of coordinates (x_j, y_j, z_j). The x_j^S, x_j^Q and x_j axes are normal to the (110) plane containing the ligands and the Fe^{3+} impurity.

From the analysis of the ENDOR data it could only be determined that the isotropic SHF constant a and the anisotropic SHF constant b of the Cl^- ligands have the same sign, but not their absolute sign. This can be determined if the sign of the fine-structure parameter B_4 is known from EPR intensity measurements at very low temperatures. No such determination has been done for the Fe^{3+} centre in NaCl (Nistor and Velter-Stefanescu 1985). However, as will be discussed later, from the interpretation of the ENDOR parameters for the ^{23}Na nuclei of the second shell of ligands it is inferred that $B_4 > 0$. This implies positive signs for the SHF parameters a and b of the first-shell Cl^- ligands.

Figure 3 shows the measured and calculated ENDOR lines of the second-shell ^{23}Na nuclei. The SHF constants, quadrupole constants and the angles describing the SHF and quadrupole tensor orientations are listed in table 1. The ENDOR spectra measured on EPR transitions with $|m_x| > \frac{1}{2}$ and $B_0 \| [100]$ were also taken into consideration in the determination of the SHF and quadrupole constants of the second shell.

From the analysis it follows only that a, b and b' have the same sign. Their sign is the same as that of the fine-structure parameter B_4. As expected for a second shell of ligands in an ionic compound (Spaeth *et al* 1992), the anisotropic SHF constant b is mainly due to the point dipole–dipole interaction between the Fe^{3+} ion and the ligand, which is positive for both ^{35}Cl and ^{37}Cl isotopes. This observation not only determines the positive sign of all SHF parameters, but also determines the sign of the fine-structure parameter as $B_4 > 0$.

The principal z axis of the SHF tensor of the second shell of cations is in the (110) plane containing Na^{II}, Cl^I and Fe^{3+}, and tilted toward the Fe^{3+}–ligand connection line by an angle Θ_S. This tilting angle is visible in figure 3 as a splitting of the outermost ENDOR lines when the crystal is turned out of the [100] direction. The principal z^Q axis of the quadrupole tensor is tilted with an angle Θ_Q, in the same (110) plane, but away from the

Fe^{3+}–ligand connecting line. A similar tensor orientation has been observed previously for the second shell of ligands surrounding other interstitial centres in alkali halides, such as Fe^{3+}_{cub} in AgCl (Garth 1965, Satoh and Slichter 1966) and H^0_i in KCl (Spaeth 1966).

4. Discussion

We have determined the SHF and quadrupole interaction constants of the nearest set (shell I) of chlorine ligands and of the second-nearest set (shell II) of sodium ligands. The absence of interacting ^{23}Na nuclei in the first shell of cation ligands, as well as the number and symmetry of the surrounding ligands, confirms the structural model of the Fe^{3+}_{cub} centre in NaCl as an Fe^{3+} ion on an interstitial site surrounded by a regular tetrahedron of four chlorine ligands and four sodium vacancies at the nearest cation sites (figure 4).

The SHF and quadrupole constants of the Fe^{3+}_{cub} centre are very similar for the first shell of chlorine ligands in both NaCl and AgCl (see table 1), which can be explained by assuming the same Fe^{3+}–Cl^- distance for both hosts. This suggests that the Fe^{3+}_{cub} centre behaves mostly as an $[FeCl_4]^-$ molecular ion embedded in the crystal lattice. It has been argued previously (Hayes *et al* 1964) that the stability of this entity can explain the formation of the interstitial Fe^{3+}_{cub} centre.

In a purely ionic model we can treat the d orbitals of the Fe^{3+} ion as an envelope function to interpret the SHF constants. As shown previously for 3d ions in alkali and alkali earth halides (Ziegler 1972, Studzinski *et al* 1984, Cases *et al* 1987), orthogonalization of this envelope function to the s and p orbitals of the first shell of ligands yields values of the isotropic and anisotropic constants that are far too low. This failure to explain the SHF constants reflects the neglect of covalency effects between Fe^{3+} and Cl^- which are expected for an $[FeCl_4]^-$ molecular ion.

The unpaired spin density in the *second* shell is due to transferred SHF interaction. One can try to estimate it in an orthogonalization model by using the wave function of the $[FeCl_4]^-$ molecular ion as an envelope function. The latter can be constructed approximately by using the experimental values of the isotropic and anisotropic SHF constant of Cl^I to determine the unpaired spin density in the 3s and 3p orbitals of Cl^- using equations (4) and (5), whereby the point dipole–dipole term b_{dd} must be taken into account (see e.g. Spaeth *et al* 1992, ch 7).

$$a(\mathrm{Cl}) = K\eta^2_{3s}|\Psi_{3s}(0)|^2 \tag{4}$$

$$b(\mathrm{Cl}) = K'\eta^2_{3p\sigma}\langle r^{-3}\rangle_{3p} \tag{5}$$

with $K = 2/3\mu_0 g_e \mu_B g_I \mu_K = 792.8$ MHz au$^3 \times g_I$ and $K' = (1/4\pi)\frac{2}{5}\mu_0 g_e \mu_B g_I \mu_K =$ 37.85 MHz au$^3 \times g_I$. For $\eta = 1$ the values are $a(\mathrm{Cl}) = 5723$ MHz and $b(\mathrm{Cl}) = 175.6$ MHz (Morton and Preston 1978).

Using the experimental values of a and $b - b_{dd}$ from table 1 with $b_{dd}/h = 0.144$ MHz for the unrelaxed lattice we obtain the unpaired spin densities in the chlorine 3s and 3p orbitals:

$$\eta^2_{3s} = 1.475 \times 10^{-3} \qquad \eta^2_{3p\sigma} = 4.834 \times 10^{-3}.$$

In the orthogonalization model the transferred isotropic SHF constant is then given by (see e.g. Spaeth *et al* 1992, ch 7)

$$a_{ov}(\mathrm{Na}) = K(\eta_{3s}\langle \mathrm{Cl}_{3s}|\mathrm{Na}_{2s}\rangle \Psi^{\mathrm{Na}}_{2s}(0) + \eta_{3p\sigma}\cos(54.7°)\langle \mathrm{Cl}_{3p\sigma}|\mathrm{Na}_{2s}\rangle \Psi^{\mathrm{Na}}_{2s}(0))^2 \tag{6}$$

with

$$\Psi^{\mathrm{Na}}_{2s}(0) = 4.8418 \text{ au}^{-3/2} \qquad \langle \mathrm{Cl}_{3s}|\mathrm{Na}_{2s}\rangle = 8.8 \times 10^{-3} \qquad \langle \mathrm{Cl}_{3p\sigma}|\mathrm{Na}_{2s}\rangle = 5.331 \times 10^{-2}.$$

In this model calculation the transfer of spin density is accomplished by the overlap integrals between the outer Cl^- and Na^+ orbitals. We obtain $a_{ov}/h = 0.14$ MHz which is in fair agreement with the experimental value of 0.218 MHz considering the crude model and the neglect of lattice relaxations. The overlap part of the anisotropic SHF interaction constant b can be estimated in a similar way:

$$b_{ov}(\mathrm{Na}) = K'(\eta_{3s}\langle \mathrm{Cl}_{3s}|\mathrm{Na}_{2p\sigma}\rangle \cos(54.7°) + \eta_{3p}\langle \mathrm{Cl}_{3p\sigma}|\mathrm{Na}_{2p\sigma}\rangle \cos(54.7°))^2 \langle r^{-3}\rangle_{2p(\mathrm{Na})} \quad (7)$$

with $\langle r^{-3}\rangle_{2p(\mathrm{Na})} = 18.1$ au^{-3}, $\langle \mathrm{Cl}_{3s}|\mathrm{Na}_{2p\sigma}\rangle = 1.352 \times 10^{-2}$, $\langle \mathrm{Cl}_{3p\sigma}|\mathrm{Na}_{2p\sigma}\rangle = 4.035 \times 10^{-2}$.

The calculation yields only a value of $b_{ov}/h = 0.002$ MHz. Thus the experimental value of $b/h = 0.181$ MHz is mainly due to the point dipole–dipole interaction of $b_{dd}/h = 0.144$ MHz. Note that a lattice relaxation of Na^+ inwards towards Fe^{3+} of about 7% would explain the experimental value of b and almost also that of a.

Table 2. Theoretical and experimental values of the SHF constants a and b (in MHz) of the second shell of cations of the Fe^{3+}_{cub} centre in NaCl and AgCl considering no lattice relaxation (for details see text).

		a/h		b/h	
Host	Nucleus	Exp.	Theor.	Exp.	Theor.
NaCl	^{23}Na	0.218	0.14	0.182	0.146
AgCl	^{109}Ag	0.174	−0.39	−0.148	−0.032

The analogous calculation of transferred hyperfine interaction for the cubic Fe^{3+} centre in AgCl gave the following results: $a_{ov}/h = -0.39$ MHz, $b_{ov}/h = -0.005$ MHz and $b_{dd} = -0.027$ MHz. The negative sign of the calculated values of a and b in AgCl in comparison to NaCl is due to the opposite sign of the nuclear g factors of ^{109}Ag and ^{23}Na. In the case of AgCl the calculation cannot explain the different signs of a and b observed in the experiment (tables 1 and 2). The calculated absolute value of a is higher than the experimental value. The calculated anisotropic part b (including b_{dd}) is far too low to explain the observed anisotropic constant. An inwards relaxation of Ag^{II} would not improve the results in contrast to NaCl. In principle it could improve b, but would make a much bigger than it is now. Also, the relaxation required would be unreasonably large. It seems that in AgCl a covalency between Cl^- and Ag^+ is present which dominates the transfer of spin density. Such a covalency effect for the transferred SHF interaction was noted previously when analysing the second-shell Ag SHF interaction of Rh^{2+} centres (Olm *et al* 1988), which were second-shell neighbours along the [100] Rh^{2+}–Cl^- bond axis. In the case of Fe^{3+} in AgCl it was determined (Satoh and Slichter 1966) that the sign of the SHF constants of the second shell is $a > 0$ and $b < 0$ thus it is thought that b is mainly due to a covalency transfer between Cl^I and Ag^{II}. In addition a spin polarization effect must be important, which causes the opposite signs of a and b. Similarly as was found for Ni^+ in CaF_2 (Studzinski *et al* 1984), the orientation of the unpaired p orbital in Cl^I along a [111] direction causes apart from a σ overlap with Ag^{2+} also a π overlap, which does not admix Ag^{II} s or p_σ orbitals, but causes an exchange polarization, which leads to SHF contributions of opposite sign. The exchange polarization effect, typical for a situation in which the ligand is in a nodal plane of the unpaired electron, is usually much bigger for the s orbitals and thus for a than for the anisotropic part (see e.g. Adrian *et al* 1985). This would also explain our observation for AgCl. Thus, the analysis of the second-shell

cation SHF interactions shows that they can be fairly well understood with an ionic model for the host crystal assuming an $[FeCl_4]^-$ molecule as a defect in NaCl, while in AgCl both a covalency as well as an exchange polarization effect play an important role.

Acknowledgments

One of the authors (S V N) is indebted to the Deutscher Akademischer Austauschdienst (DAAD) for a research scholarship and to the University of Paderborn, Fachbereich 6-Physik for their hospitality during the time the main part of this research project was performed.

References

Adrian F J, Jette A N and Spaeth J-M 1985 *Phys. Rev.* B **31** 3923
Barb D, Constantinescu S, Nistor S V and Tarina D 1990 *Hyperfine Interact.* **53** 279
Cases R, Alonso P J, Alcala R and Spaeth J-M 1987 *Cryst. Latt. Defects Amorph. Mater* **16** 289
Garth J C 1965 *Phys. Rev.* **140** A656
Hayes W, Pilbrow J and Slifkin L 1964 *J. Phys. Chem. Solids* **25** 1417
Morton J R and Preston K F 1978 *J. Magn. Reson.* **30** 577
Narayana M, Sivasankar V S and Radhakrishna S 1981 *Phys. Status Solidi* b **105** 11
Nistor S V, Ursu I and Velter–Stefanescu M 1987 *Cryst. Latt. Defects Amorph. Mater* **17** 33
Nistor S V and Velter–Stefanescu M 1985 *J. Phys. C: Solid State Phys.* **18** 397
Olm M T, Niklas J R and Spaeth J-M 1988 *Phys. Rev.* B **38** 4343
Satoh M and Slichter Ch P 1966 *Phys. Rev.* **144** 259
Sootha G D and Agarwal S K 1971 *Phys. Status Solidi* a **5** 293
Spaeth J-M 1966 *Z. Phys.* **192** 107
Spaeth J-M, Niklas J R and Bartram R H 1992 *Structural Analysis of Point Defects in Solids—An Introduction to Multiple Magnetic Resonance Spectroscopy (Springer Series in Solid State Sciences 43)* (Berlin: Springer)
Studzinski P, Casas-Gonzales J and Spaeth J-M 1984 *J. Phys. C: Solid State Phys.* **17** 5411
Ziegler H 1972 *Phys. Status Solidi* b **49** 367